Supporting Information for "Distribution, Mixing, and Transformation of a Loop Current Ring Waters: The Case of Gulf of Mexico"

Mathieu Gentil[1,2], Enric Pallàs-Sanz[1], Leo Middleton[3], Angel Ruiz-Angulo[4], Thomas Meunier[1,3,5], Giovanni Durante[1], Miguel Tenreiro[1], Sheila N. Allis Estrada[1], Julio Sheinbaum[1]

[1]Center for Scientific Research and Higher Education at Ensenada, Ensenada, Mexico
[2]Current affiliation: Aix-Marseille Univ., Université de Toulon, CNRS, IRD, MIO UM 110, Marseille, France
[3]Woods Hole Oceanographic Institution, Woods Hole, MA, USA
[4]Institute of Earth Sciences, University of Iceland, 102 Reykjavik, Iceland
[5]Laboratoire d'Océanographie Physique et Spatiale (LOPS), University of Brest, CNRS, IRD, Ifremer, IUEM, France

Contents of this file

- Text S1 to S2
- Figures S1 to S8

Description

- Text S1: The dissipation thermal variance rates (χ) (Osborn & Cox, 1972), were derived from spectra of temperature gradients (Ψ) and the Batchelor spectrum (Ψ_B) (Batchelor, 1959), through an iterative calculation as outlined by Scheifele et al. (2018):

$$\chi = \chi_{lW} + \chi_{obs} + \chi_{hW} = 6D_T \left(\int_0^{k_l} \Psi_B \, dk + \int_{k_l}^{k_u} \Psi \, dk + \int_{k_u}^{\infty} \Psi_B \, dk \right), \quad (1)$$

The iterative calculation process involves the following steps: (i) Fit the Batchelor spectrum, Ψ_B, to the observed spectrum Ψ for each iteration; (ii) Calculate χ_{obs} by integrating the observed spectrum, between the wavenumbers k_l and k_u (Fig. S2); (iii) For wavenumbers outside this range, where the observed spectrum is unreliable, we integrated Ψ_B to obtain the correction terms χ_{lW} and χ_{hW}; (iv) The factor of 6 is introduced based on the assumption of isotropic flow, and D_T is the molecular diffusivity coefficient of temperature.

- Text S2: We use the parameterization developed by Middleton et al. (2021) to estimate the dissipation rate associated with double-diffusive convection. This parameterization works by estimating the turbulent buoyancy flux $\langle w'b' \rangle$, and assuming it is in balance with the dissipation rate ε. They estimate the turbulent buoyancy flux by using an assumption of balance in the variance equation for buoyancy, following Osborn and Cox (1972). In other words, they assume that the available potential energy within the small scale turbulence is in a quasi-steady state, so the primary balance is between the diapycnal buoyancy flux:

$$\Phi_d = \left\langle \frac{(\kappa_T + \kappa_S)}{2b_z^*} |\nabla b|^2 + \frac{(\kappa_T - \kappa_S)}{2b_z^*} \nabla b \cdot \nabla s_p \right\rangle, \quad (2)$$

and the turbulent buoyancy flux $\langle w'b' \rangle$, averaged over the space between observations. Here b_z^* is the adiabatically resorted buoyancy profile, and s_p denotes the 'spice', which is defined using a linear equation of state as $s_p = g\alpha T + g\beta S$ for the purposes of the parameterization.

The diapycnal buoyancy flux Φ_d is estimated from observations by assuming that spice has a steeper spectral slope for its power spectrum than does buoyancy. So the buoyancy gradient is estimated using observations of N^2, and we assume a spectral slope of k^{-1} for the power spectrum of spice on sub-observational scales. The magnitude of the spice gradient at the overturning scale $|\nabla s_p|$ is estimated by fitting a power spectrum between each pair of observations using a two-point correlation along an isopycnal. The assumed slope of the spectrum can be altered to account for lesser degrees of stirring of spice. Details on the iterative method used to calculate Φ_d can be found in Middleton et al. (2021). This method assumes double-diffusive convection is present, as it relies on the second term of Φ_d which is purely double diffusive (Notice for equal molecular diffusivities κ_T and κ_S, this term dissapears). The parameterization also assumes an anti-correlation between ∇b and ∇s_p on overturning scales, which amounts to an assumption that double-diffusive convection is present.

- Figure S1 shows the parameters used for the optimal multiparameter analysis: conservative temperature (θ), absolute salinity (S_A) , dissolved oxygen (O_2), and potential vorticity (PV). The water mass types are defined as (quasi) continuous lines in the parameter space considering the most characteristic values of the water masses involved. We used the CTD cast data to find the characteristic parameter values in the entire profile from the Loop Current Ring (LCR) center (red line) and those taken outside of the LCR (blue line), based on the range defined in Portela et al. (2018). We focused on complete profiles because we aim to examine the transitional waters between the pure LCR or Caribbean waters and the mature forms of the Gulf waters, such as Gulf Common Water, as glider samples are collected near the LCR boundary.

- Figure S2 shows temperature gradient spectra (Ψ) of randomly selected vertical profile sections. Integration limits for χ estimation are clearly marked by red circles (k_{min}) and red squares (k_{max}). Data points falling below the noise spectrum (red dotted line) have been excluded to prevent contamination by instrumental noise. Additionally, high-wavenumber data that deviate from the theoretical Batchelor spectrum (dashed lines) have been removed to avoid fine-scale contamination.

- Figure S3 shows the histogram of the Ozmidov length scale, ($L_O = (\varepsilon/N^3)^{1/2}$), which is a metric of the size of the turbulent overturns. The mean size of the turbulent overturns is 1.67 m for all data (grey) and 0.17 m for data below the mixed layer (orange).

- Figure S4 shows the glider's cross-section of conservative temperature, absolute salinity and density anomaly, revealing interleaving layers of warmer, saltier water with cooler, fresher layers. These layers are steeper than isopycnals suggesting that advection or stirring by the mesoscale eddy may be shaping these structures (Meunier et al., 2019), supported by evidence that submesoscale processes primarily drive spice distribution (Fig. S6).

- Figure S5 describes the distribution of temperature staircases in the water column. Double-diffusive convection (DDC) may be characterized by a Turner Angle of -45/-90 rad^{-1} and 45/90 rad^{-1} for the diffusive convection (DC) and salt fingering (SF) conditions, respectively. The Turner angle shows two areas susceptible to DDC conditions, (i) the thermohaline intrusions (blue square), and (ii) salt-fingers favourable conditions (red square). In the blue square, spice anomalies are greater than density anomalies (panel c), in average by a factor 2, which is a typical pattern of thermohaline intrusions or layering (Meunier et al., 2019). These structures present some thermohaline staircases reaching up to 5 m of vertical length (panel d), which are smaller than the spice anomalies (up to 20 m). A second area, below 200 m depth, shows SF conductive conditions (red square in panel b). As shown in panel e, spice anomalies are smaller or compensated by density anomalies. High-resolution temperature profiles from the thermistor reveal indistinct thermohaline staircases (panel f).

- Figure S6 shows the averaged power spectral density of spice anomalies variance, calculated within the isopycnal range from 24.7 kg m^{-3} to 26.1 kg m^{-3}. The slope of $k^{-2.2}$ at high wavenumbers range $10^{-4.5} < k_h < 10^{-3.5}$ m^{-1} (wavelengths 3-30 km) is slightly steeper than the expected k^{-2} for quasigeostrophic turbulence. This suggests that spice anomalies are stirred around a coherent vortex, as observed in a similar structure by Meunier et al. (2019). Furthermore, the flatter slope $k^{-2.2}$ observed at high wavenumbers, compared to the typical enstrophy cascading in two-dimensional turbulence (k^{-3}), indicates that the spice distribution in the LCR is primarily driven by submesoscale processes.

- Figure S7 shows shipboard-averaged measurements from the R/V Pelican across the eddy. The stratification is stronger than the vertical shear (by an order of magnitude), resulting in a high Richardson number ($Ri > 1$), which indicates a dynamically stable water column. Additionally, the potential vorticity (PV) remains positive, suggesting that conditions are not conducive to symmetric instabilities ($PV * f < 0$).

- Figure S8 shows the buoyancy Reynolds number (R_{eb}) estimated from the vertical microstructure profiler, the glider-microstructure and the DDC parameterization from Middleton et al. (2021). R_{eb} is calculated as the ratio of the dissipation rates, which promotes vertical overturns, to the potential energy of stratification, which suppresses these overturns. A threshold for the buoyancy Reynolds number is ∼10; values below this threshold generally indicate that diapycnal turbulent mixing is suppressed (Stillinger et al., 1983; Shih et al., 2005; Ivey et al., 2008; Bouffard & Boegman, 2013). A large number of estimates, ranging from ∼63% to 77%, occurred under conditions where $Re_b < 10$, regardless of the measurement platform. This suggests that stratification suppresses shear-productions in most cases, indicating that turbulent fluxes are predominantly driven by DDC. However, a bimodal distribution is observed for vertical profiler and glider estimates, with a peak in the turbulent regime $Re_b > 10$, mainly induced by intense mixing in the surface mixed layer. The bimodal distribution is not captured by double-diffussive convection parameterization ($Re_{b_{Pred}}$), because it fails to represent shear-driven mixing or internal wave breaking.

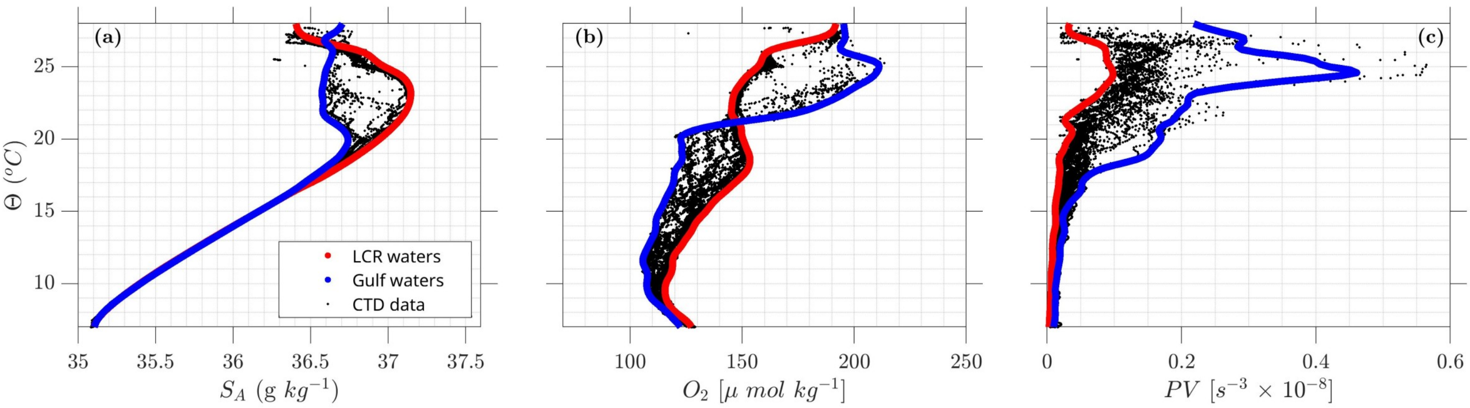

Figure S1. Water mass types definition in the parameter space (thick lines) used for the optimal multiparameter analysis. The blue line represents the Gulf waters outside the LCR and the red line shows the LCR's core waters. Black dots are the CTD data used to separate the profiles inside from outside the eddy. (a) θ-S_A, (b) θ-O_2, and (c) θ-PV diagrams.

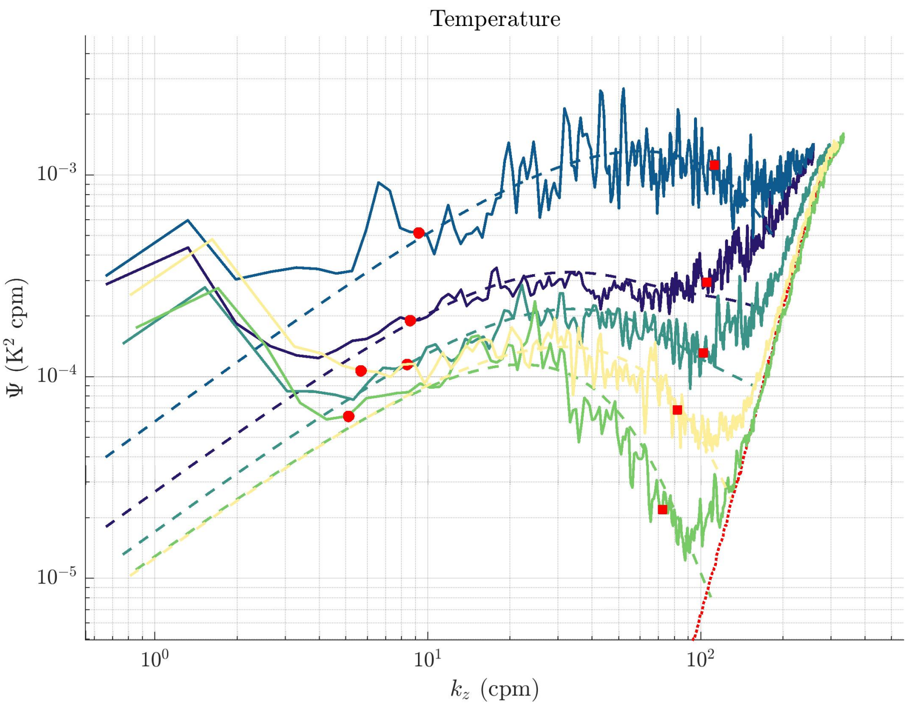

Figure S2. Temperature gradient spectra (Ψ) of randomly selected vertical profile sections from the thermistor. The spectra of temperature gradients were integrated between k_{min} (red circles) and k_{max} (red squares). The dotted lines represent the corresponding empirical spectra obtained through fitting to the Batchelor spectrum. The red dotted line indicates the thermistor's theoretical noise curve.

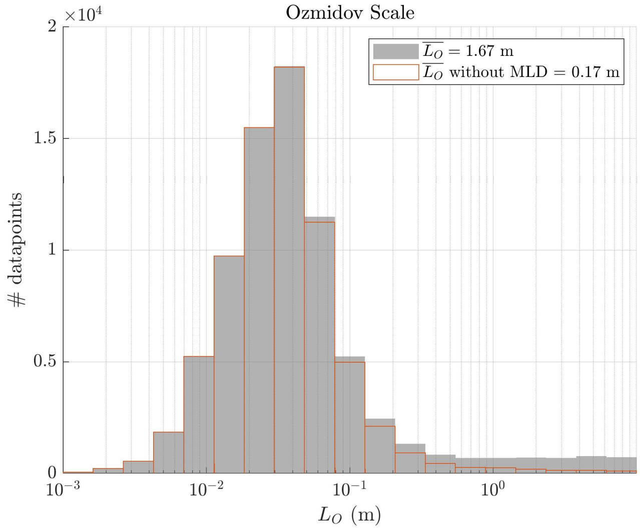

Figure S3. Histogram of the Ozmidov length scale (L_O; m), with all data in grey and only data below the mixed-layer in orange. For both datasets, mean values are indicated as $\overline{L_O}$.

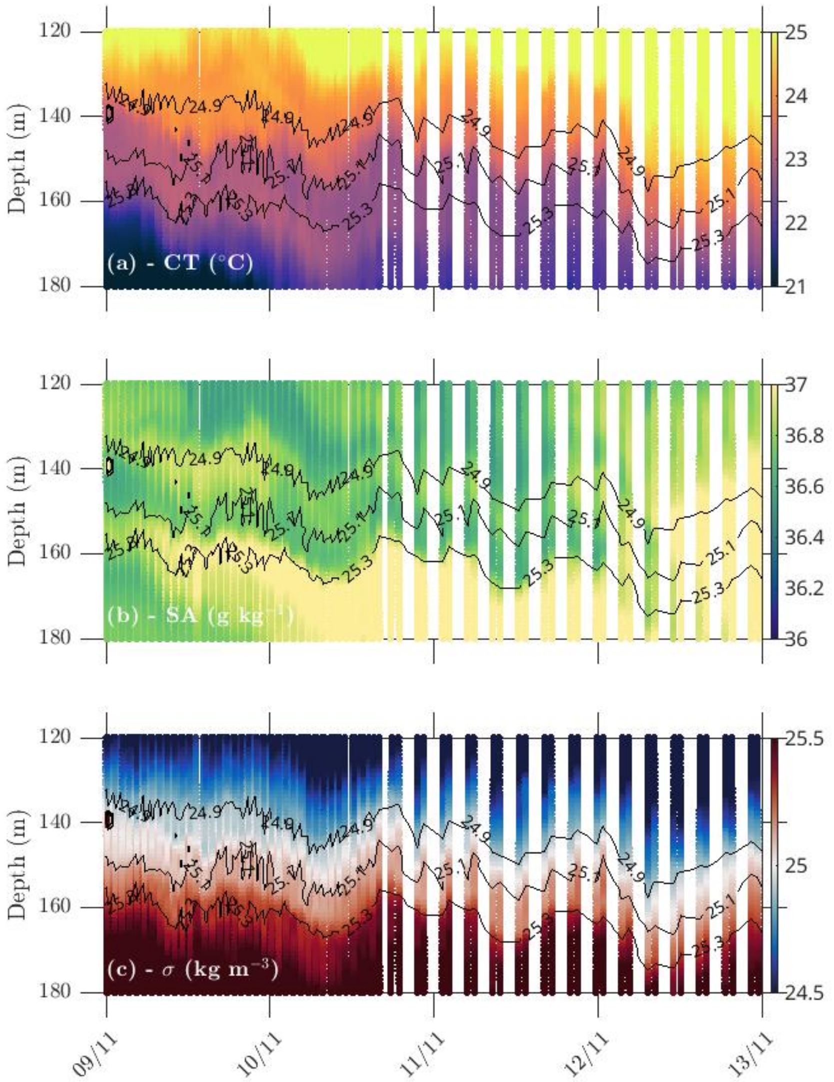

Figure S4. Glider cross-section of (a) conservative temperature, (b) absolute salinity, and (c) density anomaly in the layering region (eddy periphery). Isopycnal layers are represented by black contours.

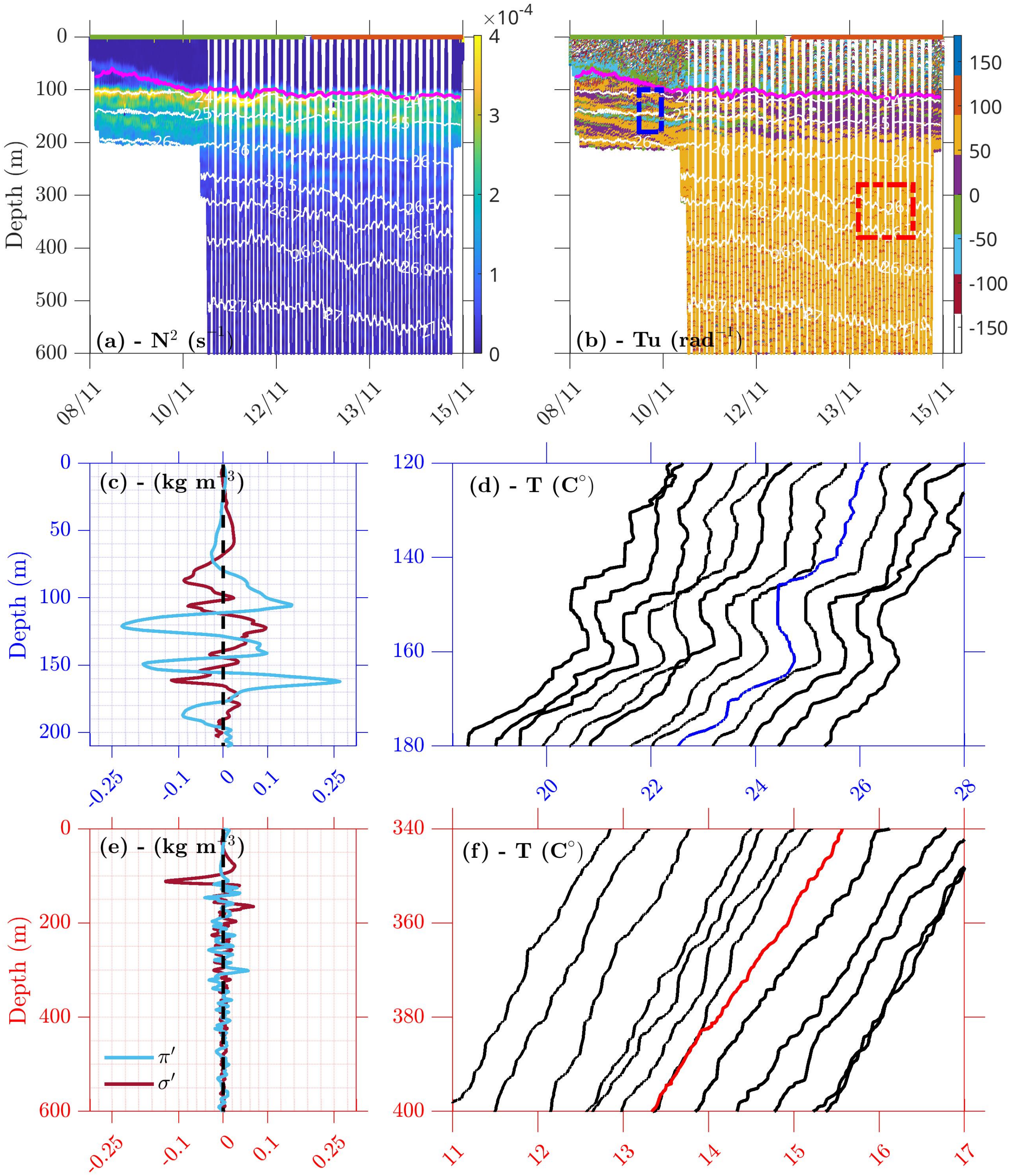

Figure S5. Glider section of (a) squared Brunt-Väisälä frequency and (b) Turner angle, where regions that are susceptible to double-diffusive convection are indicated by values of -45/-90 rad^{-1} (double-convection: light blue), and 45/90 rad^{-1} (salt-finger: yellow). Regions of thermohaline intrusions (blue square) and salt finger conditions (red square) were highlighted. (c) and (e) are one of the spice (blue) and density (red) anomaly profiles from the blue and red squares in (b) respectively. (d) and (f) are selected temperature profiles (presented as relative temperature, shifted by and offset of 0.5°C) recorded by the FP07 fast thermistor in the blue and red squares in (b), respectively. The blue and red profiles are those represented in (c) and (e), respectively.

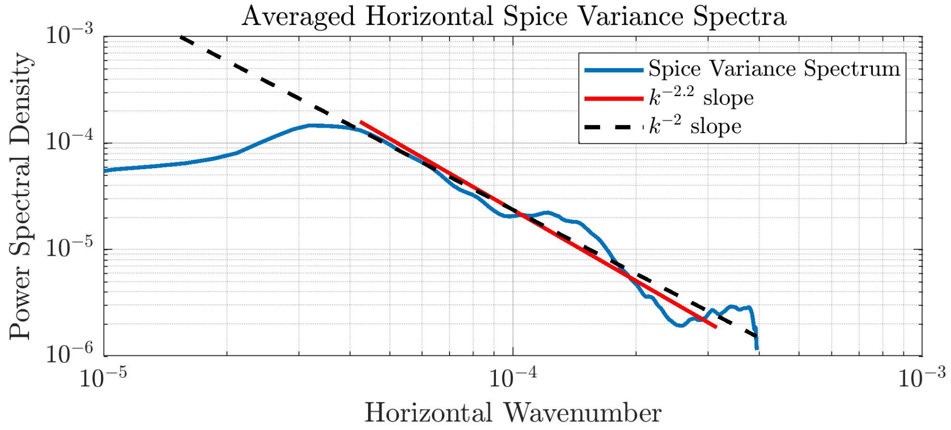

Figure S6. Power spectral density in isopycnal coordinates of spice variance anomalies. Spectra are averaged over the isopycnal range from 24.7 kg m^{-3} to 26.1 kg m^{-3}. The red line represents the linear fit of the spectra $10^{-4.5} < k_h < 10^{-3.5}$ m^{-1} in the wavenumber range (wavelengths of 3-30 km), and the k^{-2} slope is marked by the dashed black line.

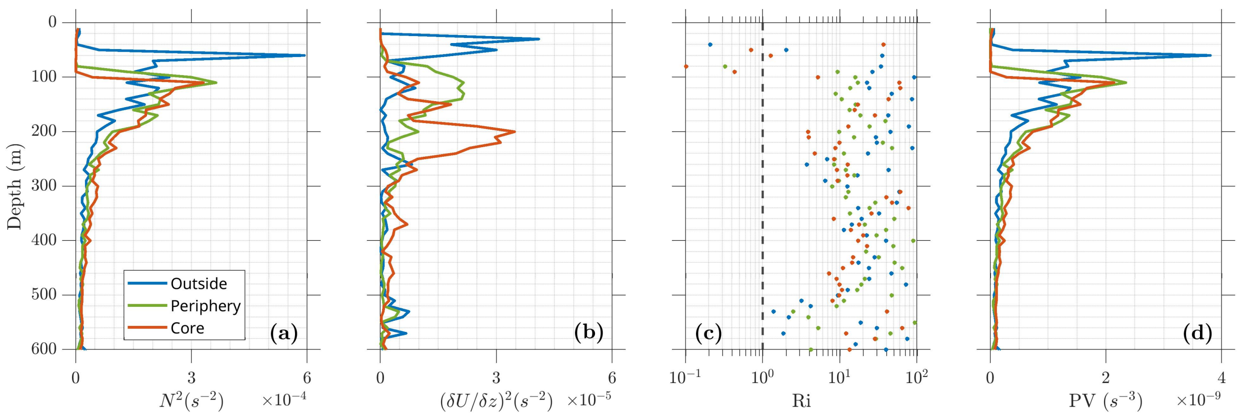

Figure S7. Shipboard averaged measurements from the R/V Pelican across the eddy: (a) squared Brunt-Väisälä frequency, (b) vertical shear from L-ADCP, (c) Richardson number, and (d) potential vorticity. The blue, green, and orange lines and colored dots represent measurements taken at different locations: outside the eddy, at its periphery, and at its core, respectively.

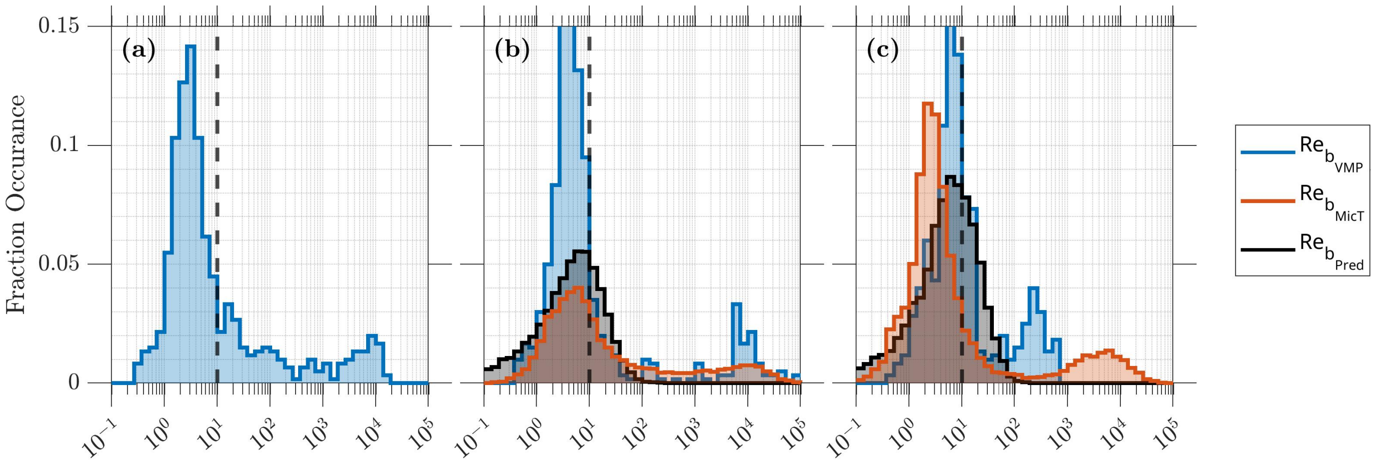

Figure S8. (a, b, c) Log-histograms comparing predicted buoyancy Reynolds number ($Re_{b_{Pred}}$) from double-diffusive convection parameterization (Middleton et al., 2021), with estimates from microstructure ($Re_{b_{MicT}}$) and VMP ($Re_{b_{VMP}}$), covering areas outside the eddy (a), its periphery (b), and center (c), respectively.

References

Batchelor, G. K. (1959). Small-scale variation of convected quantities like temperature in turbulent fluid part 1. general discussion and the case of small conductivity. *Journal of fluid mechanics*, *5*(1), 113–133.

Bouffard, D., & Boegman, L. (2013). A diapycnal diffusivity model for stratified environmental flows. *Dynamics of Atmospheres and Oceans*, *61*, 14–34.

Ivey, G., Winters, K., & Koseff, J. (2008). Density stratification, turbulence, but how much mixing? *Annu. Rev. Fluid Mech.*, *40*, 169–184.

Meunier, T., Sanz, E. P., Tenreiro, M., Ochoa, J., Angulo, A. R., & Buckingham, C. (2019). Observations of layering under a warm-core ring in the gulf of mexico. *Journal of Physical Oceanography*, *49*(12), 3145–3162.

Middleton, L., Fine, E., MacKinnon, J., Alford, M., & Taylor, J. (2021). Estimating dissipation rates associated with double diffusion. *Geophysical Research Letters*, *48*(15), e2021GL092779.

Osborn, T. R., & Cox, C. S. (1972). Oceanic fine structure. *Geophysical Fluid Dynamics*, *3*(4), 321–345.

Portela, E., Tenreiro, M., Pallàs-Sanz, E., Meunier, T., Ruiz-Angulo, A., Sosa-Gutiérrez, R., & Cusí, S. (2018). Hydrography of the central and western gulf of mexico. *Journal of Geophysical Research: Oceans*, *123*(8), 5134–5149.

Scheifele, B., Waterman, S., Merckelbach, L., & Carpenter, J. R. (2018). Measuring the dissipation rate of turbulent kinetic energy in strongly stratified, low-energy environments: A case study from the arctic ocean. *Journal of Geophysical Research: Oceans*, *123*(8), 5459–5480.

Shih, L. H., Koseff, J. R., Ivey, G. N., & Ferziger, J. H. (2005). Parameterization of turbulent fluxes and scales using homogeneous sheared stably stratified turbulence simulations. *Journal of Fluid Mechanics*, *525*, 193–214.

Stillinger, D., Helland, K., & Van Atta, C. (1983). Experiments on the transition of homogeneous turbulence to internal waves in a stratified fluid. *Journal of Fluid Mechanics*, *131*, 91–122.